Computational and Structural Biotechnology Journal 19 (2021) 4472–4485

COMPUTATIONAL AND STRUCTURAL BIOTECHNOLOGY JOURNAL

journal homepage: www.elsevier.com/locate/csbj

Identification of subtypes correlated with tumor immunity and immunotherapy in cutaneous melanoma

Qian Liu [a,b,c], Rongfang Nie [a,b,c], Mengyuan Li [a,b,c], Lin Li [a,b,c], Haiying Zhou [d], Hui Lu [d,*], Xiaosheng Wang [a,b,c,*]

[a] Biomedical Informatics Research Lab, School of Basic Medicine and Clinical Pharmacy, China Pharmaceutical University, Nanjing 211198, China
[b] Cancer Genomics Research Center, School of Basic Medicine and Clinical Pharmacy, China Pharmaceutical University, Nanjing 211198, China
[c] Big Data Research Institute, China Pharmaceutical University, Nanjing 211198, China
[d] Department of Orthopedics, The First Affiliated Hospital, College of Medicine, Zhejiang University, Hangzhou 310003, China

ARTICLE INFO

Article history:
Received 25 February 2021
Received in revised form 4 August 2021
Accepted 4 August 2021
Available online 06 August 2021

Keywords:
Melanoma
Tumor immune microenvironment
Immune subtypes
Clustering analysis
Immunotherapy

ABSTRACT

Because immune checkpoint inhibitors (ICIs) are effective for a subset of melanoma patients, identification of melanoma subtypes responsive to ICIs is crucial. We performed clustering analyses to identify immune subtypes of melanoma based on the enrichment levels of 28 immune cells using transcriptome datasets for six melanoma cohorts, including four cohorts not treated with ICIs and two cohorts treated with ICIs. We identified three immune subtypes (Im-H, Im-M, and Im-L), reproducible in these cohorts. Im-H displayed strong immune signatures, low stemness and proliferation potential, genomic stability, high immunotherapy response rate, and favorable prognosis. Im-L showed weak immune signatures, high stemness and proliferation potential, genomic instability, low immunotherapy response rate, and unfavorable prognosis. The pathways highly enriched in Im-H included immune, MAPK, apoptosis, calcium, VEGF, cell adhesion molecules, focal adhesion, gap junction, and PPAR. The pathways highly enriched in Im-L included Hippo, cell cycle, and ErbB. Copy number alterations correlated inversely with immune signatures in melanoma, while tumor mutation burden showed no significant correlation. The molecular features correlated with favorable immunotherapy response included immune-promoting signatures and pathways of PPAR, MAPK, VEGF, calcium, and glycolysis/gluconeogenesis. Our data recapture the immunological heterogeneity in melanoma and provide clinical implications for the immunotherapy of melanoma.

1. Background

Recently, immune checkpoint inhibitors (ICIs) have achieved success in treating various malignancies [1]. In particular, melanoma is the cancer type in which ICIs have achieved the earliest and greatest success for its high tumor mutation burden (TMB) [2,3]. Nevertheless, only a subset of melanoma patients displayed an active response to ICIs [4]. To improve the efficacy of ICIs, certain biomarkers associated with the response to ICIs have been identified, including PD-L1 expression [5], DNA mismatch repair deficiency [6], and TMB [7]. In general, the T cell-inflamed tumor microenvironment (TME) may facilitate a response to ICIs [8]. Thus, differentiating high-immune-response tumors from low-immune-response tumors may aid the selection of cancer patients responsive to ICIs. To this end, we have developed an immunogenomic profiling-based unsupervised machine learning method for the identification of high- and low-immune-response tumor subtypes [9]. Several studies have proved that this method is effective in the identification of immune subtypes of cancers [10].

In this study, we identified immune subtypes of cutaneous melanoma based on the enrichment levels of 28 immune cells by

Abbreviations: **TCGA**, The Cancer Genome Atlas; **ICIs**, immune checkpoint inhibitors; **TIME**, tumor immune microenvironment; **TME**, tumor microenvironment; **HLA**, human leukocyte antigen; **EMT**, epithelial-mesenchymal transition; **TMB**, tumor mutation burden; **SCNAs**, somatic copy number alterations; **ssGSEA**, single-sample gene-set enrichment analysis; **NK**, natural killer; **MDSC**, myeloid-derived suppressor cell; **FDR**, false discovery rate; **OS**, overall survival; **DSS**, disease-specific survival; **DMFS**, distant-metastasis free survival; **WGCNA**, weighted gene co-expression network analysis; **GSEA**, gene-set enrichment analysis; **HRD**, homologous recombination deficiency; **GO**, gene ontology.

* Corresponding authors at: Department of Orthopedics, The First Affiliated Hospital, College of Medicine, Zhejiang University, Hangzhou 310003, China (H. Lu); Biomedical Informatics Research Lab, School of Basic Medicine and Clinical Pharmacy, China Pharmaceutical University, Nanjing 211198, China (X. Wang).

E-mail addresses: huilu@zju.edu.cn (H. Lu), xiaosheng.wang@cpu.edu.cn (X. Wang).

https://doi.org/10.1016/j.csbj.2021.08.005

performing clustering analyses. In six different datasets, we consistently identified three immune subtypes of melanoma with high, medium, and low immunity, respectively. We comprehensively characterized the molecular and clinical landscapes of these melanoma subtypes. Moreover, we associated the immune subtypes with the response to ICIs. Our identification of the immune subtypes of melanoma may provide new insights into the biology of this cancer type and potential clinical application for cancer immunotherapy.

2. Methods

2.1. Datasets

We obtained four gene expression profiling datasets for cutaneous melanoma, including TCGA-melanoma [11] from the genomic data commons data portal (https://portal.gdc.cancer.gov/), and GSE65904 [12,13], GSE98394 [14], and GSE53118 [15,16] from the NCBI gene expression omnibus (https://www.ncbi.nlm.nih.gov/geo/). For TCGA-melanoma, we also downloaded its somatic mutation and copy number alteration profiling data from the genomic data commons data portal (https://portal.gdc.cancer.gov/). Moreover, we generated two gene expression profiling datasets for cutaneous melanoma in which the clinical data for ICI treatment are available. One dataset (termed ICI-R-melanoma) was generated by combining five different RNA-Seq datasets (RSEM normalized), including the Allen cohort [17], Hugo cohort [18], Nathanson cohort [19], Riaz cohort [20], and Snyder cohort [21]. Another (termed ICI-M-melanoma) was a microarray dataset from a previous publication [22]. In addition, we downloaded a single-cell RNA sequencing (scRNA-seq) dataset (GSE72056 [23]) for cutaneous melanoma from the GEO. The scRNA-seq (SMART-seq2 [24]) dataset was gene expression profiles in 4485 single cells from 18 human cutaneous melanomas, which contained 1235 tumor cells, 2643 immune cells, 64 endothelial cells, 60 cancer-associated fibroblasts (CAFs), and 483 unclassified cells. A description of these datasets is shown in Supplementary Table S1.

2.2. Single-sample gene-set enrichment analysis

We scored the enrichment level of an immune signature, pathway, or phenotypic feature in a tumor sample by using the single-sample gene-set enrichment analysis (ssGSEA) of its gene set [25]. The ssGSEA outputs the enrichment score of a gene set in a sample based on gene expression profiles. The gene sets representing immune signatures, pathways, or phenotypic features are shown in Supplementary Table S2.

2.3. Identification of immune subtypes of melanoma

We used hierarchical clustering to identify immune subtypes of melanoma based on the ssGSEA scores of 28 immune cell types, including CD56-bright natural killer (NK) cells, effector memory CD4 T cells, eosinophil, CD56-dim NK cells, type 17T helper cells, activated B cells, monocytes, memory B cells, activated CD4 T cells, type 2T helper cells, plasmacytoid dendritic cells, neutrophils, macrophages, effector memory CD8 T cells, myeloid-derived suppressor cell (MDSC), immature B cells, T follicular helper cells, NK cells, immature dendritic cells, mast cells, type 1T helper cells, activated dendritic cells, central memory CD4 T cells, gamma delta T cells, central memory CD8 T cells, regulatory T cells, activated CD8 T cells, and NK T cells [26].

2.4. Evaluation of tumor immune score and purity

We utilized ESTIMATE [27] to evaluate tumor immune score based on immune gene expression signatures. The immune score, which represents the tumor immune infiltration level, is the fraction of immune cells in bulk tumor. We also evaluated tumor purity by ESTIMATE, which is the proportion of tumor cells in bulk tumor. ESTIMATE defines tumor purity as a cosine function of the sum of immune and stromal scores. Thus, tumor purity is likely to be inversely proportional to immune scores.

2.5. Survival analysis

We used Kaplan–Meier curves to compare the survival time (ten years except five years in ICI-R-melanoma) and the log-rank test to assess the significance of survival time differences.

2.6. Pathway analysis

We used GSEA [28] to identify the KEGG [29] pathways significantly upregulated in one class versus another class based on the differentially expressed genes between both classes with a threshold of adjusted *P*-value < 0.05. The differentially expressed genes were identified using a threshold of adjusted *P*-value (false discovery rate (FDR)) < 0.05 and fold change (FC) of mean expression levels > 1.5. In addition, we used WGCNA [30] to identify the gene modules highly enriched in the immune subtypes and immunotherapy responsive and non-responsive groups of melanoma and displayed the representative gene ontology (GO) for each gene module.

2.7. Logistic regression model

We used the logistic regression model to compare the contribution of TMB and SCNAs in predicting high-immune-score (upper third) versus low-immune-score (bottom third) melanomas. In the logistic regression analysis, the R function "glm" was used to fit the binary model, and the R function "lm.beta" in the R package "QuantPsyc" was utilized to calculate the standardized regression coefficients (β values).

2.8. Evaluation of TMB and somatic copy number alterations

We defined a tumor sample's TMB as the total number of its somatic mutations. We used GISTIC2 [31] to calculate arm- and focal-level somatic copy number alterations (SCNAs) in the tumor with the input of "SNP6" files, which were downloaded from the genomic data commons data portal (https://portal.gdc.cancer.gov/). From the publication by Knijnenburg et al [32], we obtained HRD scores (aneuploidy levels) of TCGA cancers.

2.9. Combination of different gene expression profiling datasets

We merged the six gene expression profiling datasets for melanoma using the "merge" function in the R package "base". We adjusted fored batch effects and normalized combined data using the "normalizeBetweenArrays" function in the R package "limma."

2.10. Statistical analysis

When comparing two classes of data, we used Mann–Whitney *U* test for non-normally distributed data and Student's *t* test for normally distributed data. When evaluating the correlation between two groups of data, we used Spearman's correlation for non-normally distributed data and Pearson's correlation for normally-distributed data. We used Fisher's exact test to assess

the association between two categorical variables. The Benjamini-Hochberg method [33] was used for adjusting for multiple tests. We performed all statistical analyses in the R programming environment (version 4.0.2).

3. Results

3.1. Identification of immune subtypes of melanoma

Based on the ssGSEA scores of 28 immune cell types, we hierarchically clustered melanomas in six datasets (TCGA-melanoma, GSE65904, GSE98394, GSE53118, ICI-R-melanoma, and ICI-M-melanoma). Consistently, we obtained three clear clusters in these datasets, which had high, medium, and low levels of immunity, respectively (Fig. 1). We termed the three immune subtypes Im-H, Im-M, and Im-L, which represent the high, medium, and low-immunity subtypes, respectively. We further demonstrated that there were significantly different levels of immune signatures among Im-H, Im-M, and Im-L based on additional analyses. The immune scores followed the pattern: Im-H > Im-M > Im-L, in all six datasets (one-tailed Mann–Whitney *U* test, $P < 0.001$) (Fig. 2A). By contrast, tumor purity had an opposite trend: Im-H < Im-M < Im-L ($P < 0.001$) (Supplementary Fig. S1). HLA genes, which encode MHC proteins, play important roles in the regulation of the immune system. We observed a number of HLA genes differentially expressed among the immune subtypes and following the expression pattern: Im-H > Im-M > Im-L (one-way ANOVA test, $P < 0.001$) (Fig. 2B and Supplementary Fig. S2). The interferon (type I and II) response scores also followed the pattern: Im-H > Im-M > Im-L ($P < 0.01$) (Fig. 2C). The pathological slides data for TCGA-melanoma showed that Im-H and Im-L had the highest and lowest percentages of lymphocyte infiltration, respectively ($P = 0.014$) (Fig. 2D). Collectively, these results confirmed the markedly distinct tumor immune microenvironment (TIME) among the three subtypes of melanoma.

The 28 immune cell types are involved in both immunostimulatory and immunosuppressive function, which were likely consistently upregulated in Im-H while downregulated in Im-L respectively (Fig. 1). Nevertheless, we observed that the ratios of immunostimulatory to immunosuppressive signatures (CD8+/CD4 + regulatory T cells, pro-/anti-inflammatory cytokines, and M1/M2 macrophages) still followed the pattern: Im-H > Im-M > Im-L (two-tailed Student's *t* test, $P < 0.05$) (Fig. 2E). Interestingly, PD-L1 had significantly different expression levels among the three subtypes: Im-H > Im-M > Im-L (one-way ANOVA test, $P < 0.05$) (Fig. 2F). Also, the ratios of CD8 + T cell/PD-L1 followed the same pattern: Im-H > Im-M > Im-L ($P < 0.05$) (Fig. 2F). Overall, these results suggest that Im-H and Im-L had the highest and lowest anti-tumor immune response among the three subtypes, respectively.

3.2. Clinical and phenotypic characteristics of the immune subtypes

In TCGA-melanoma, Im-H displayed a better overall survival (OS) prognosis than Im-M and Im-L (log-rank test, $P < 0.05$), and Im-M had better OS than Im-L ($P = 0.003$) (Fig. 3A). In GSE65904, Im-H showed better disease-specific survival (DSS) and distant metastasis-free survival (DMFS) than Im-M and Im-L ($P < 0.02$), while there was no significant difference in DSS or DMFS between Im-M and Im-L ($P > 0.5$) (Fig. 3A). In GSE98394, Im-L displayed worse OS and DMFS than Im-H and Im-M ($P < 0.001$), while there was no significant difference in OS or DMFS between Im-H and Im-M ($P > 0.5$) (Fig. 3A). In GSE53118, Im-M had better OS than Im-L ($P < 0.01$), while Im-H showed no significant OS difference with Im-M ($P = 0.9$) and Im-L ($P = 0.283$) (Fig. 3A). In ICI-R-melanoma, Im-L showed worse OS than Im-H and Im-M ($P < 0.01$), while there was no significant difference in OS between Im-H and Im-M ($P = 0.7$) (Fig. 3A). Collectively, these results indicated that Im-H and Im-L were likely to have the best and worst survival prognosis among the three immune subtypes of melanoma, respectively. This indication suggests a positive association between immune signatures and survival prognosis in melanoma, consistent with previous findings in many other cancer types, including gastric cancer [34], head and neck squamous cell cancer [35], and triple-negative breast cancer [36]. To check whether the survival difference among these immune subtypes is associated with their distinct TIME, we compared the survival prognosis between high-immune-score (upper third) and low-immune-score (bottom third) melanomas. We observed that high-immune-score melanomas had a significantly better survival prognosis than low-immune-score melanomas (Fig. 3B), confirming that the TIME significantly impacts survival prognosis in melanoma.

We compared several phenotypic features between Im-H and Im-L melanomas. These phenotypic features included tumor stemness, proliferation potential, and epithelial-mesenchymal transition (EMT). Notably, Im-H had significantly lower stemness scores than Im-L in five of the six datasets, except that in GSE98394 where Im-H had significantly higher stemness scores than Im-L; Im-H had significantly lower proliferation potential scores than Im-L in four datasets (Fig. 3C). Overall, these results suggest that the elevated anti-tumor immunity is likely to inhibit tumor progression in melanoma. Nevertheless, Im-H tended to have significantly higher EMT signature scores than Im-L (Fig. 3C), suggesting a more enriched stromal microenvironment in Im-H than in Im-L melanomas.

3.3. Molecular characteristics of the immune subtypes

3.3.1. Pathways

GSEA [28] identified numerous KEGG [29] pathways highly enriched in Im-H and Im-L (Fig. 4A) based on the significantly upregulated genes in Im-H versus Im-L (Student's *t* test, FDR < 0.05, FC > 1.5) (Supplementary Table S3). As expected, many of the pathways highly enriched in Im-H were immune relevant, including cytokine-cytokine receptor interactions, chemokine signaling, NK cell-mediated cytotoxicity, intestinal immune network for IgA production, graft-versus-host disease, allograft rejection, antigen processing and presentation, primary immunodeficiency, T and B cell receptor signaling, Jak-STAT signaling, Toll-like receptor signaling, NOD-like receptor signaling, complement and coagulation cascades, cytosolic DNA-sensing, Fc gamma R-mediated phagocytosis, Fc epsilon RI signaling, and RIG-I-like receptor signaling (Fig. 4A). Besides, many cancer-associated pathways were highly enriched in Im-H, including MAPK signaling, apoptosis, calcium signaling, VEGF signaling, cell adhesion molecules, focal adhesion, and gap junction (Fig. 4A). Indeed, the positive association between some of these pathways and immune activities has been revealed in previous studies, including apoptosis [34], calcium signaling [34], focal adhesion [34], MAPK [37], and VEGF [34]. The pathways highly enriched in Im-L included adherens junction, insulin signaling, arginine and proline metabolism, purine metabolism, and ErbB signaling. The negative association between ErbB signaling and tumor immunity has been indicated in a previous study [35].

3.3.2. Genomic features

In TCGA-melanoma, TMB was significantly higher in Im-M than in Im-H and Im-L (one-tailed Mann–Whitney *U* test, $P < 0.001$), while it showed no significant difference between Im-H and Im-L (two-sided Mann–Whitney *U* test, $P = 0.80$) (Fig. 4B). It suggests that TMB has no significant impact on the TIME in TCGA-

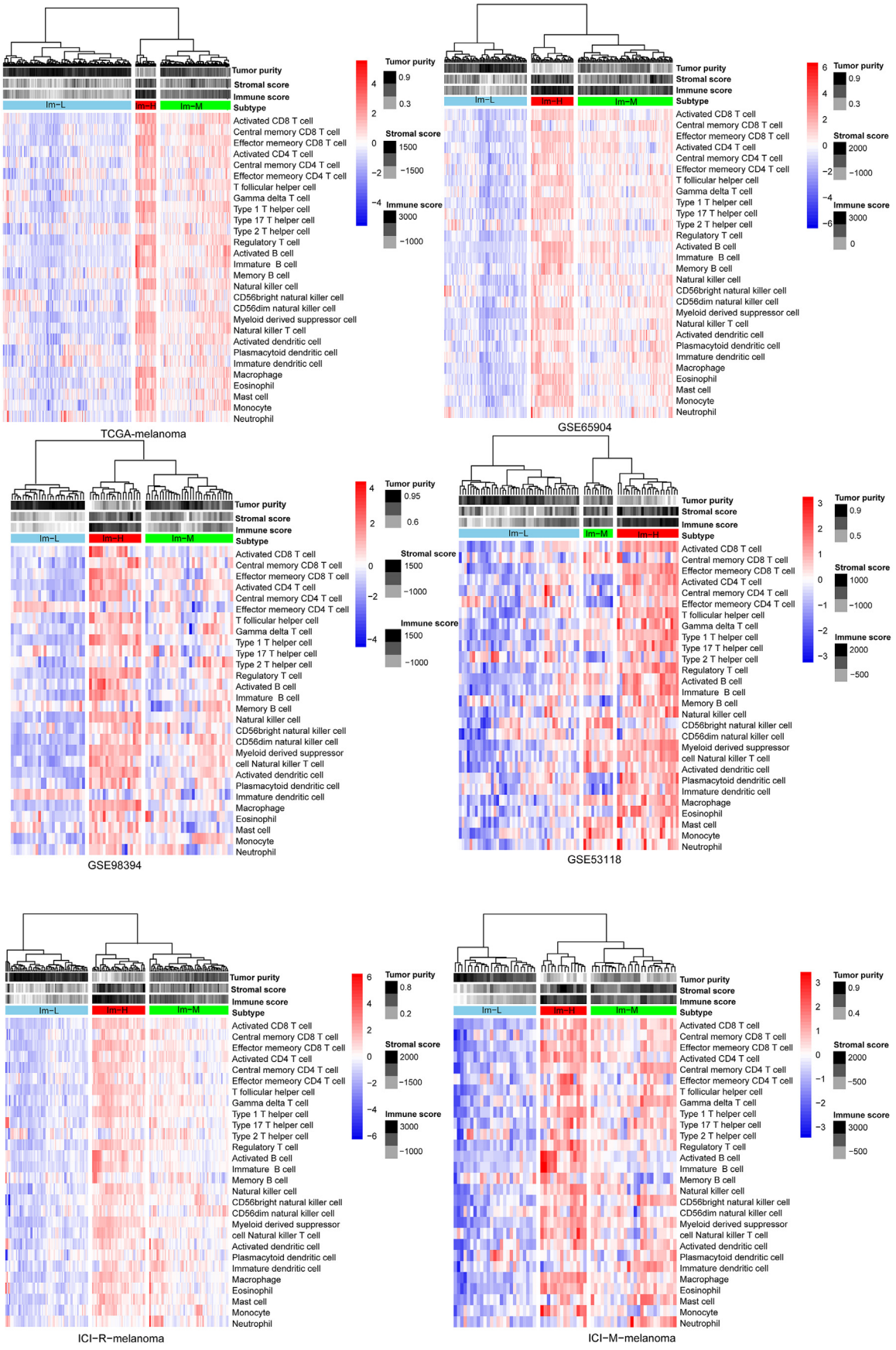

Fig. 1. Identification of immune subtypes of melanoma based on the enrichment scores of 28 immune cell types by hierarchical clustering. In six datasets, three clusters were clearly identified: Im-H, Im-M, and Im-L, representing the high, medium, and low-immunity subtypes, respectively.

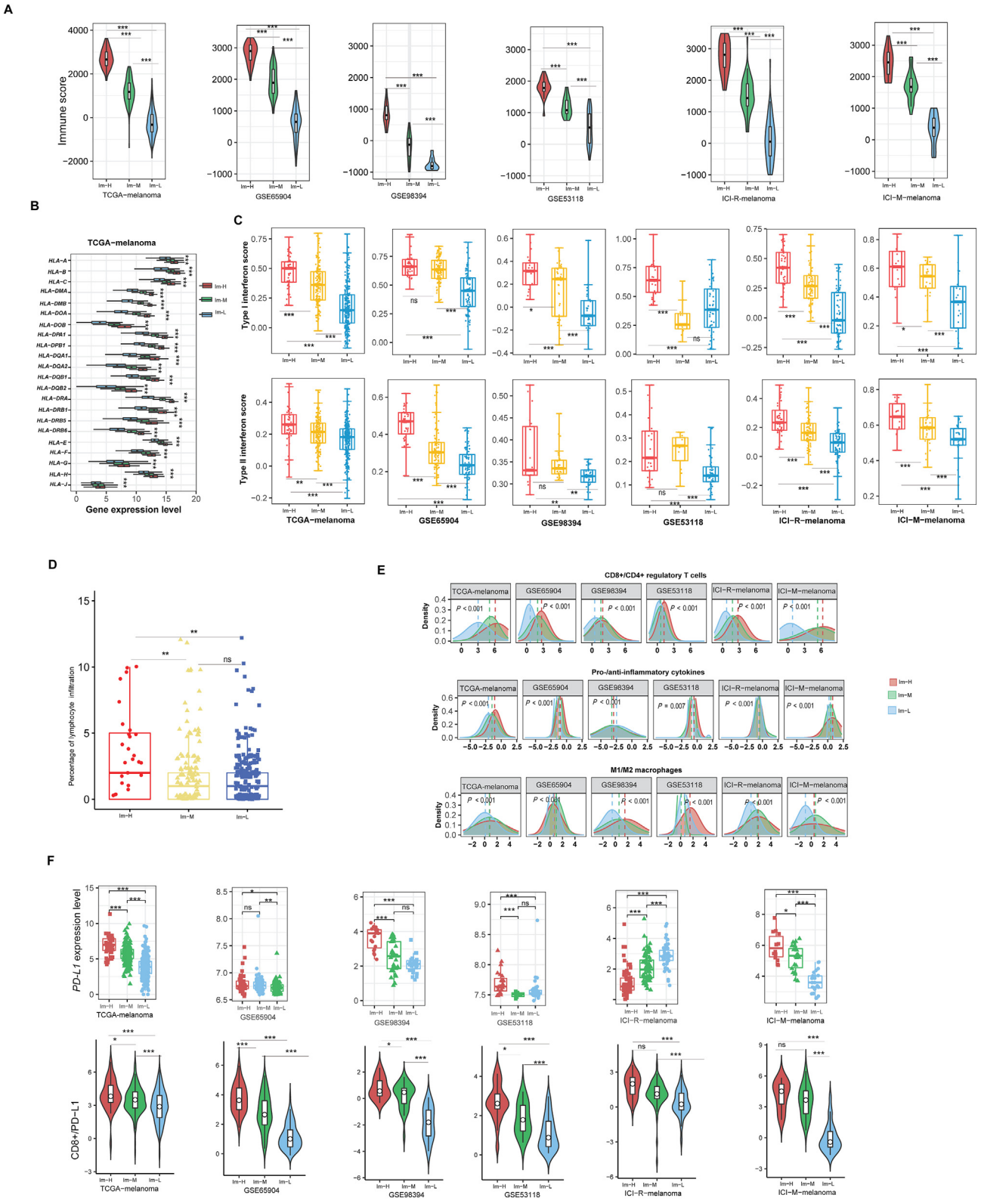

Fig. 2. Comparisons of immune signatures among the three immune subtypes of melanoma. Immune scores evaluated by ESTIMATE [36] (A), expression levels of HLA genes (B), interferon (type I and II) response scores (C), percentages of lymphocyte infiltration (D), ratios of immunostimulatory/immunosuppressive signatures (E), and PD-L1 expression levels and the ratios of CD8 + T cell/PD-L1 were compared among the three immune subtypes of melanoma. * $P < 0.1$, ** $P < 0.01$, *** $P < 0.001$, ^{ns} $P \geq 0.1$. It also applies to the following figures.

melanoma. This finding is in line with a recent study showing that high TMB may inhibit immune infiltration in melanoma [38]. It is also in agreement with our recent study demonstrating that TMB and anti-tumor immune response is cancer type-dependent [3]. However, we found that SCNAs, known as large-scale genomic instability, displayed a significant association with the TIME in melanoma. For instance, the scores of homologous recombination deficiency (HRD), which contributes to large-scale genomic insta-

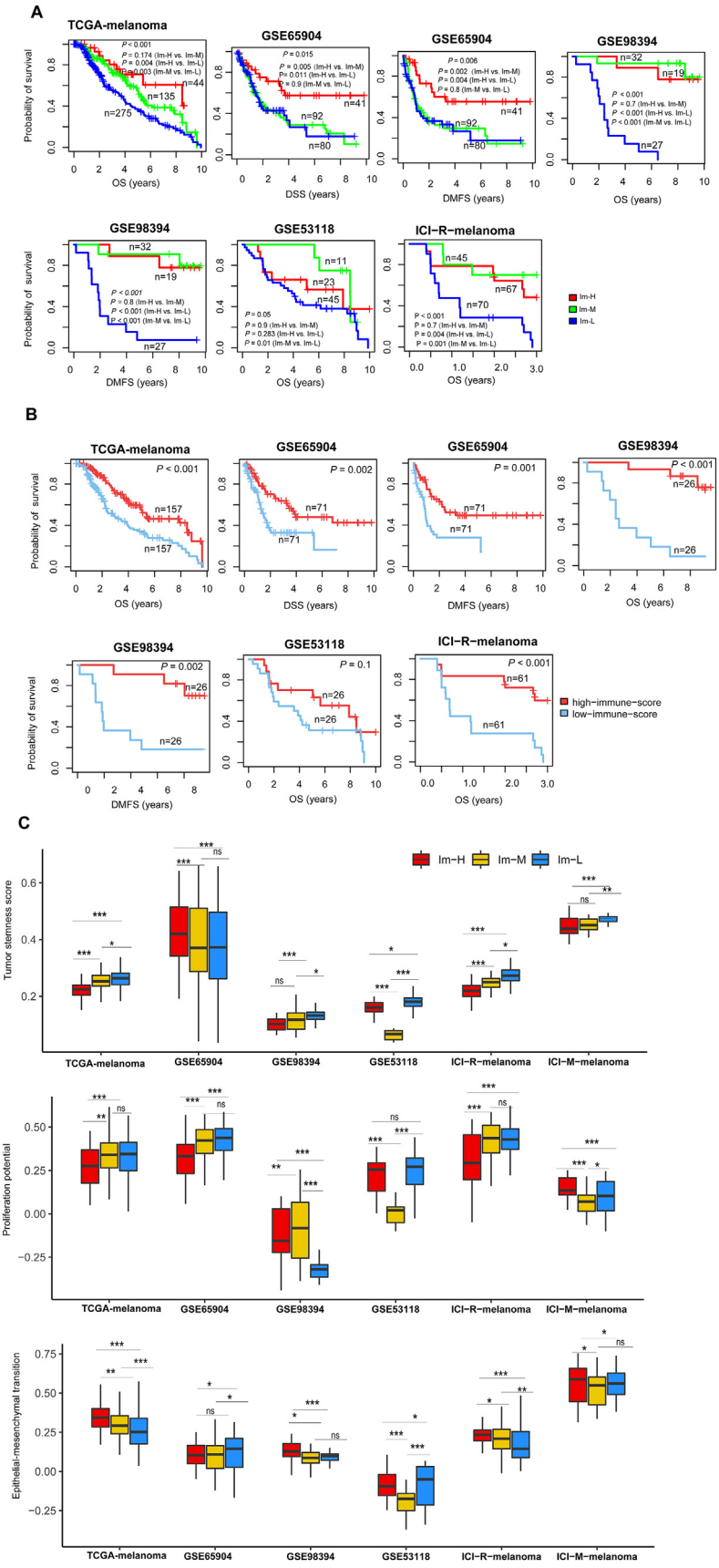

Fig. 3. Comparisons of clinical and phenotypic features among the three immune subtypes of melanoma. Comparisons of survival prognosis among the three immune subtypes (A) and between high-immune-score (upper third) and low-immune-score (bottom third) melanomas (B). The log-rank test *P*-values are shown. C. Comparisons of the scores of tumor stemness, proliferation potential, and epithelial-mesenchymal transition (EMT) among the three immune subtypes. The one-tailed Mann–Whitney *U* test *P*-values are indicated. OS: overall survival; DSS: disease-specific survival; DMFS: distant-metastasis free survival.

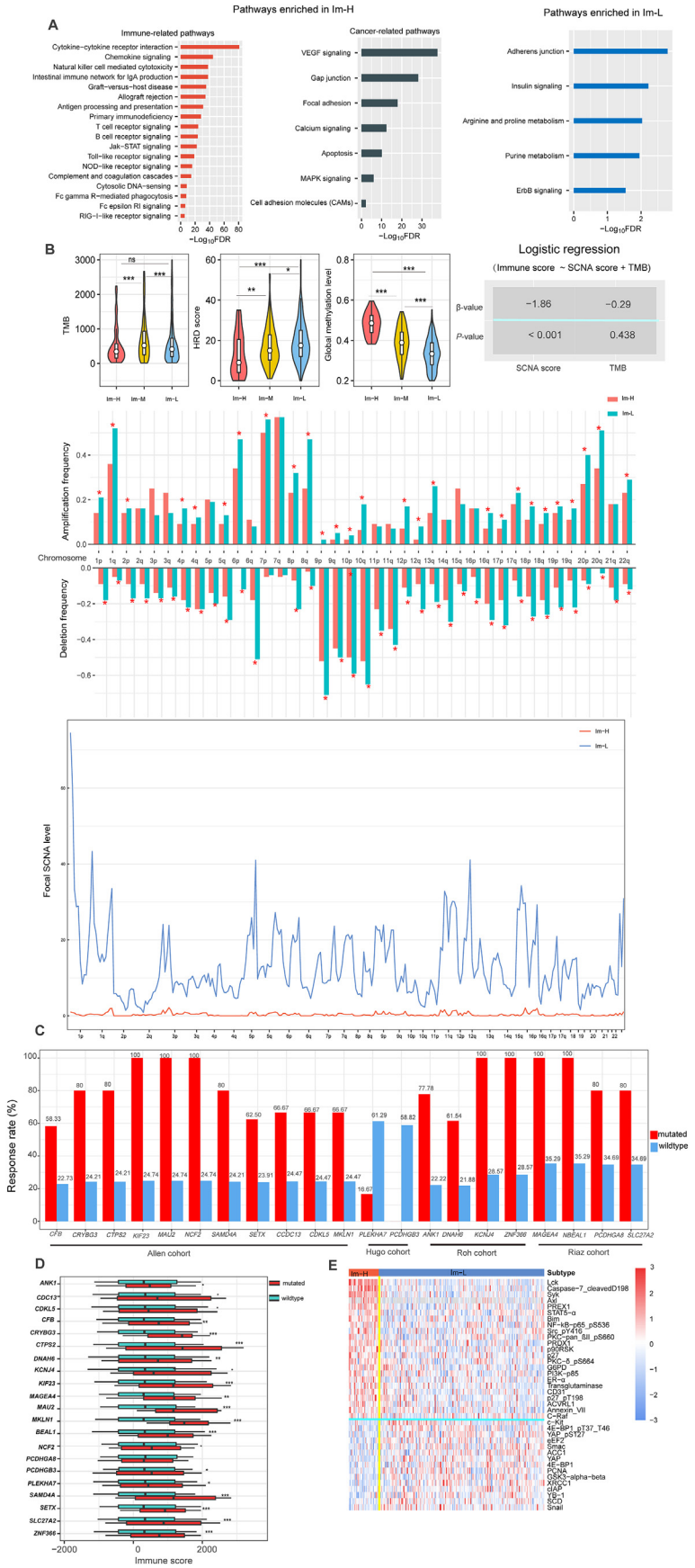
A
Pathways enriched in Im-H
Immune-related pathways
Cytokine−cytokine receptor interaction
Chemokine signaling
Natural killer cell mediated cytotoxicity
Intestinal immune network for IgA production
Graft−versus−host disease
Allograft rejection
Antigen processing and presentation
Primary immunodeficiency
T cell receptor signaling
B cell receptor signaling
Jak−STAT signaling
Toll−like receptor signaling
NOD−like receptor signaling
Complement and coagulation cascades
Cytosolic DNA−sensing
Fc gamma R−mediated phagocytosis
Fc epsilon RI signaling
RIG−I−like receptor signaling
−Log10FDR
Cancer-related pathways
VEGF signaling
Gap junction
Focal adhesion
Calcium signaling
Apoptosis
MAPK signaling
Cell adhesion molecules (CAMs)
−Log10FDR
Pathways enriched in Im-L
Adherens junction
Insulin signaling
Arginine and proline metabolism
Purine metabolism
ErbB signaling
−Log10FDR
B
TMB
HRD score
Global methylation level
Im-H
Im-M
Im-L
Logistic regression
(Immune score ~ SCNA score + TMB)
β-value
P-value
−1.86
−0.29
< 0.001
0.438
SCNA score
TMB
Amplification frequency
Deletion frequency
Chromosome
Focal SCNA level
C
Response rate (%)
mutated
wildtype
CFB
CRYBG3
CTPS2
KIF23
MAU2
NCF2
SAMD4A
SETX
CCDC13
CDKL5
MKLN1
PLEKHA7
PCDHGB3
ANK1
DNAH6
KCNJ4
ZNF366
MAGEA4
NBEAL1
PCDHGA8
SLC27A2
Allen cohort
Hugo cohort
Roh cohort
Riaz cohort
D
Immune score
E
Subtype
Lck
Caspase−7_cleavedD198
Syk
ZAP
PREX1
STAT5−α
Bim
NF−κB−p65_pS536
Src_pY416
PKC−pan_BII_pS660
PRDX1
p90RSK
B2M
PKC−δ_pS664
G6PD
PI3K−p85
ER−α
Transglutaminase
CD31
p27_pT198
ACVRL1
Annexin_VII
C−Raf
c−Kit
4E−BP1_pT37_T46
YAP_pS127
SF3B3
Smac
ACC1
YAP
4E−BP1
PCNA
GSK3−alpha−beta
XRCC1
cIAP
YB−1
SCD
Snail

bility [36], followed the pattern: Im-H < Im-M < Im-L (one-tailed Mann–Whitney *U* test, $P < 0.05$) (Fig. 4B). Im-L had significant higher arm-level amplification and deletion frequencies and focal-level amplification and deletion levels than Im-H ($P < 0.001$) (Fig. 4B). These results indicated that SCNAs reduced anti-tumor immune response in melanoma, consistent with previous findings [39]. To further compare the impact of TMB and SCNAs on the TIME, we built a logistic regression model with two predictors (TMB and SCNA score [36]) to predict high-immune-score (upper third) versus low-immune-score (bottom third) melanomas. As expected, the SCNA score was a significant negative predictor ($P < 0.001$, $\beta = -1.86$), while TMB had no significant contribution in the prediction ($P = 0.438$, $\beta = -0.29$) (Fig. 4B). In addition, a recent study showed that the reduced DNA methylation facilitated tumor immune evasion [40]. Consistent with that finding, the global methylation levels in TCGA-melanoma [40] followed the pattern: Im-H > Im-M > Im-L ($P < 0.001$) (Fig. 4B).

3.3.3. Mutation profiles

We found 380 genes whose mutation frequencies were significantly different between Im-H and Im-L in TCGA-melanoma (Fisher's exact test, $P < 0.05$) (Supplementary Table S4). Among them, BRAF had the highest mutation rate (68.2%) in Im-H versus 47.4% in Im-L ($P = 0.014$, odds ratio (OR) = 2.37). EP400 was another gene displaying a significantly higher mutation rate in Im-H than in Im-L (31.8% versus 14.6%; $P = 0.008$, OR = 2.72). B2M also showed a significantly higher mutation rate in Im-H than in Im-L (9.1% versus 1.5%; $P = 0.015$, OR = 6.68). Among the 380 genes differentially mutated between Im-H and Im-L, 21 had significant correlations of their mutations with better responses to ICIs in at least a melanoma cohort. The 21 genes included *CFB*, *CRYBG3*, *CTPS2*, *KIF23*, *MAU2*, *NCF2*, *SAMD4A*, *SETX*, *CCDC13*, *CDKL5*, and *MKLN1* in the Allen cohort [17], *PLEKHA7* and *PCDHGB3* in the Hugo cohort [18], *MAGEA4*, *NBEAL1*, *PCDHGA8*, and *SLC27A2* in the Riaz cohort [20], and *ANK1*, *DNAH6*, *KCNJ4*, and *ZNF366* in the Roh cohort (Fig. 4C). Notably, 20 of the 21 genes had significantly higher mutation rates in Im-H than in Im-L, and their mutations correlated with higher immune scores (Fig. 4D).

3.3.4. Protein expression profiles

We analyzed protein expression profiles in the subtypes in TCGA-melanoma, whereas protein expression profiles were not available for the other datasets. In spite of this limitation in data availability, we reported related findings from TCGA-melanoma due to their relevance. We found 38 proteins whose expression levels were significantly different between Im-H and Im-L in TCGA-melanoma (two-tailed Student's *t* test, $P < 0.05$) (Fig. 4E). Among them, 23 were more highly expressed in Im-H than in Im-L, including Axl, Caspase-7_cleavedD198, Syk, Lck, PREX1, STAT5-α, Bim, NF-kB-p65_pS536, Src_pY416, PKC-pan_βII_pS660, PRDX1, p90RSK, p27, PKC-δ_pS664, G6PD, PI3K-p85, ER-α, Transglutaminase, CD31, p27_pT198, ACVRL1, Annexin_VII, and C-Raf. Notably, most of these proteins had significant positive expression correlations with immune scores (Spearman's correlation, $P < 0.05$) (Supplementary Fig. S3). Among these proteins upregulated in Im-H, Caspase-7 is a major promoter of apoptosis [41], which correlates positively with anti-tumor immune response [37]. In contrast, 15 proteins had higher expression levels in Im-L than in Im-H, including c-Kit, 4E-BP1_pT37_T46, YAP_pS127, eEF2, Smac, ACC1, 4E-BP1, YAP, XRCC1, YB-1, PCNA, GSK3-α-β, Snail, SCD, and cIAP. Most of them showed significant negative expression correlations with immune scores (Supplementary Fig. S3). Notably, YAP_pS127 and YAP are involved in the Hippo signaling pathway, which is a negative regulator of anti-tumor immune response [9,42]. Thus, their upregulation should inhibit anti-tumor immune response, consistent with our results. Snail, another protein upregulated in Im-L, has been shown to play a role in tumor immunosuppression [43]. XRCC1 and PCNA, which function in DNA damage repair [44], were upregulated in Im-L probably because the high genomic instability stimulated their expression in this subtype.

3.4. Associations of immune subtypes and immune signatures with immunotherapy response in melanoma

In ICI-R-melanoma, the rate of response to ICIs followed the pattern: Im-H (44.4%) > Im-M (31.3%) > Im-L (18.6%) (Fig. 5A). In ICI-M-melanoma, the rate followed the pattern: Im-M (57.9%) > Im-H (42.9%) > Im-L (8.0%). These results indicated that Im-L had the lowest reponse rate to ICIs in melanoma. To further explore the association between the TIME and immunotherapy response in melanoma, we compared immune signature scores between the responsive (complete or partial response) group and the non-responsive group in ICI-R-melanoma and ICI-M-melanoma. We found that immune scores were higher in the responsive group in both ICI-R-melanoma ($P = 0.082$) and ICI-M-melanoma ($P = 0.003$) (Fig. 5B). Most of the 28 immune cell types for clustering analyses displayed significantly higher enrichment levels in the responsive group ($P < 0.1$) (Fig. 5C). Numerous HLA genes showed significantly higher expression levels in the responsive group than in the non-responsive group ($P < 0.1$) (Supplementary Fig. S4). PD-L1 was more highly expressed in the responsive group in both ICI-R-melanoma ($P = 0.038$) and ICI-M-melanoma ($P = 0.017$) (Fig. 5D). The ratios of immunostimulatory/immunosuppressive signatures (CD8+/CD4 + regulatory T cells, CD8+/PD-L1, and M1/M2 macrophages) were significantly higher in the responsive group ($P < 0.1$) (Fig. 5E). Overall, these results indicate a significant association between the TIME and immunotherapy response in melanoma. In contrast, the stemness scores were significantly higher in the non-responsive group ($P < 0.05$) (Fig. 5F). It indicates that tumor stemness may promote immunotherapy resistance.

3.5. Identification of pathways associated with immunotherapy response in melanoma

GSEA [29] identified numerous pathways associated with the upregulated genes in the responsive group versus the non-responsive group (FDR < 0.25, FC > 1.5) in ICI-R-melanoma with a threshold of adjusted *P*-value < 0.25 (Fig. 6A). As expected, many immune-related pathways were in the list, including T and B cell receptor signaling, cytokine-cytokine receptor interaction, NK cell mediated cytotoxicity, antigen processing and presentation, chemokine signaling, NOD-like receptor signaling, and Jak-STAT signaling. Again, these results indicate a significant positive association between the strength of immune signatures and the response to immunotherapy in melanoma. In addition, several

Fig. 4. Molecular features of the immune subtypes of melanoma. A. KEGG [29] pathways highly enriched in Im-H and Im-L identified by GSEA [20]. B. Comparisons of tumor mutation burden (TMB), homologous recombination deficiency (HRD) scores, and global methylation levels among the three immune subtypes in TCGA-melanoma; prediction of high-immune-score (upper third) versus low-immune-score (bottom third) melanomas using TMB and somatic copy number alteration (SCNA) score by the logistic regression model; comparisons of arm-level amplification and deletion frequencies and focal-level amplification and deletion levels between Im-H and Im-L melanomas. C. 21 genes showing significant correlations of their mutations with better responses to immune checkpoint inhibitors (ICIs) in at least a melanoma cohort. D. 20 genes which have significantly higher mutation rates in Im-H than in Im-L and whose mutations correlate with better responses to ICIs and higher immune scores. E. 38 proteins differentially expressed between Im-H and Im-L in TCGA-melanoma (two-tailed Student's *t* test, $P < 0.05$).

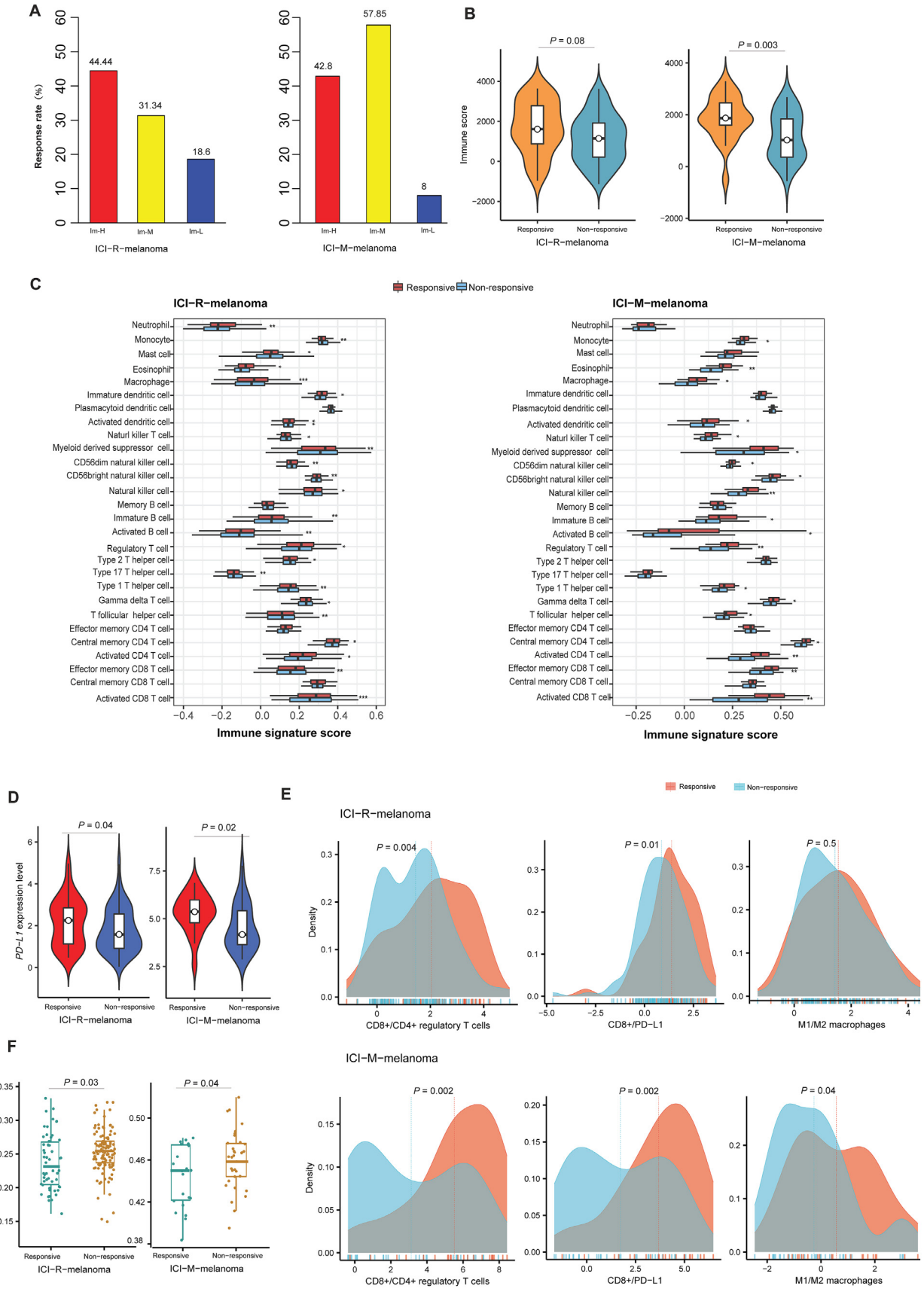

Fig. 5. Associations of immune subtypes and immune signatures with immunotherapy response in melanoma cohorts treated with immune checkpoint inhibitors. A. Comparisons of the rate of response to ICIs among the three immune subtypes. Comparisons of immune scores (B), enrichment levels of 28 immune signatures (C), PD-L1 expression levels (D), ratios of immunostimulatory/immunosuppressive signatures (E), and stemness scores (F) between the responsive and non-responsive melanomas.

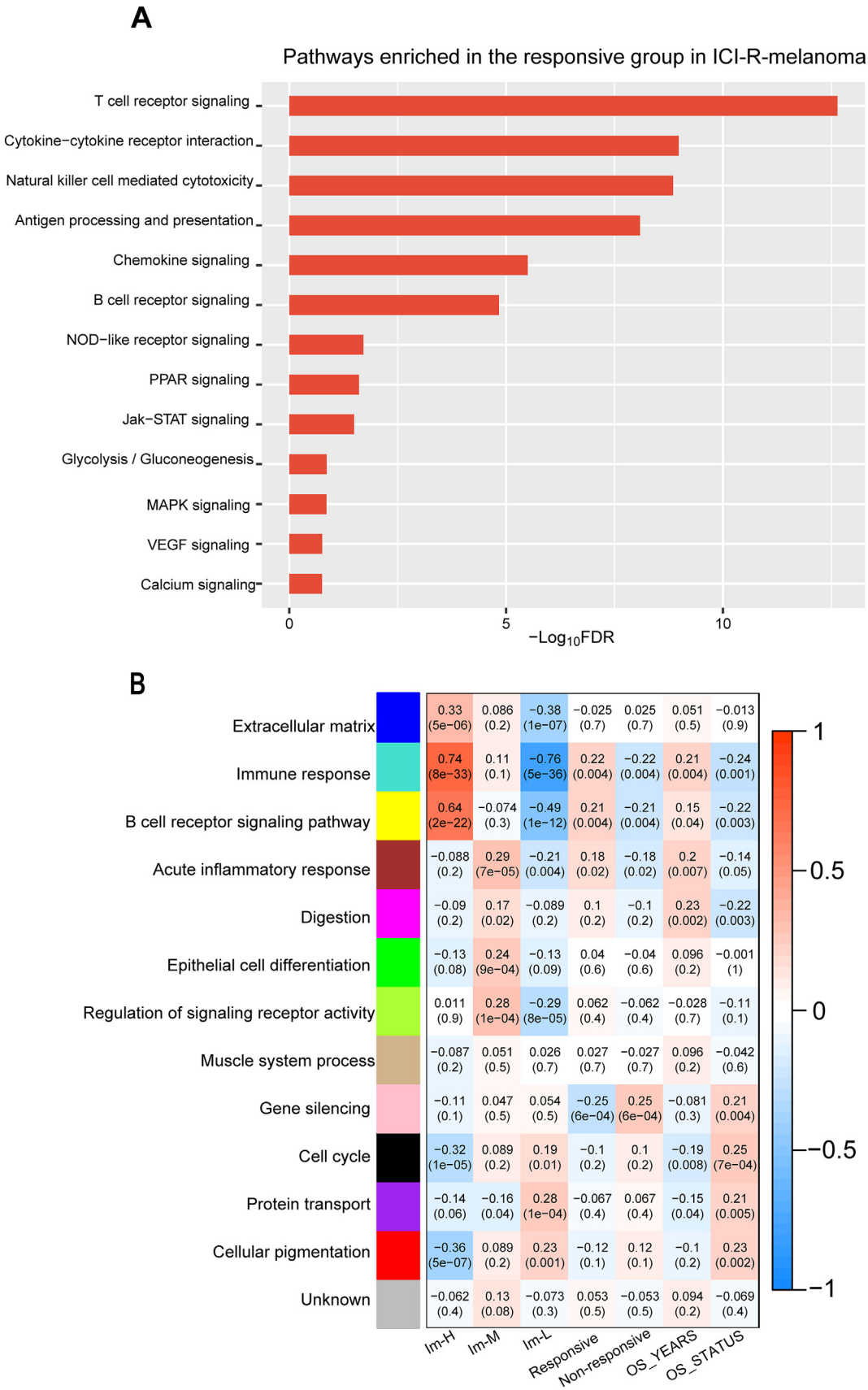

Fig. 6. Pathways and gene ontology associated with immunotherapy response in melanoma. A. Pathways upregulated in the responsive versus non-responsive melanomas. B. 12 gene modules (indicated in different colors) that significantly differentiated melanomas by immune subtype, immunotherapy response, or overall survival (OS) prognosis identified by WGCNA [30]. The representative gene ontology for gene modules, correlation coefficients, and *P*-values (in parenthesis) are shown.

cancer-associated pathways were in the list, including PPAR signaling, glycolysis/gluconeogenesis, MAPK signaling, VEGF signaling, and calcium signaling (Fig. 6A). Among them, the glycolysis/gluconeogenesis pathway has been shown to have a positive correlation with immunotherapy response in melanoma [41].

In ICI-R-melanoma, WGCNA [30] identified 12 gene modules that significantly differentiated melanomas by immune subtype, immunotherapy response, or OS prognosis (Fig. 6B). The representative GO terms for the gene modules (indicated in turquoise, yellow, and blue color) upregulated in Im-H while downregulated in Im-L included immune response, B cell receptor signaling pathway, and extracellular matrix. The representative GO terms for the gene modules (indicated in brown, magenta, green, and green yellow color) enriched in Im-M included acute inflammatory response, digestion, epithelial cell differentiation, and regulation of signaling receptor activity. The representative GO terms for the gene modules (indicated in black, purple, and red color) upregulated in Im-L while downregulated in Im-H included cell cycle, protein transport, and cellular pigmentation. These results indicate that the immune and stromal signatures are enriched in Im-H and that the cell cycle pathway is enriched Im-L. The significant association between cell cycle and anti-tumor immunosuppression has been demonstrated in a previous study [45].

Three gene modules (indicated in turquoise, yellow, and brown color) were upregulated in the responsive group versus non-responsive group, whose representative GO terms were immune response, B cell receptor signaling pathway, and acute inflammatory response, respectively (Fig. 6B). Again, these results suggest that the active TIME promotes immunotherapy response in melanoma. As expected, the three gene modules were associated with better OS prognosis in melanoma, consistent with their high enrichment in the responsive group. In contrast, the pink gene module was upregulated in the non-responsive group versus responsive group, which was associated with worse OS prognosis. Its representative GO term was gene silencing. In addition, the black gene module, which was upregulated in Im-L and downregulated in Im-H but not differentially enriched between the responsive and non-responsive groups, was associated with worse OS prognosis. Its representative GO term was cell cycle. It indicates that in the setting of insignificant difference in immunotherapy response, the elevated cell cycle activity may lead to worse outcomes in melanoma by inhibiting anti-tumor immune response.

3.6. Comparisons of molecular and phenotypic features between the melanomas treated and those untreated with ICIs

To explore how ICIs have altered the molecular and phenotypic features of melanoma, we compared immune signatures, stromal signatures, tumor purity, stemness, proliferation potential, and intratumor heterogeneity (ITH) between the melanomas treated with ICIs and those untreated with ICIs. We found that immune signature (CD8 + T cells and immune cytolytic activity) scores were significantly higher in ICIs-treated melanomas ($P < 0.05$) (Fig. 7A). Meanwhile, PD-L1 expression levels were also upregulated in this cohort ($P < 0.001$). However, the ratios of immunostimulatory to immunosuppressive signatures (CD8 + T cells/PD-L1 and M1/M2 macrophages) were significantly higher in ICIs-treated melanomas (Fig. 7A). These results suggest that the use of ICIs promotes the formation of immunostimulatory TME in melanoma.

Stromal scores were also significantly higher in ICIs-treated melanomas ($P < 0.001$) (Fig. 7B). In contrast, tumor purity was significantly lower in ICIs-treated melanomas ($P < 0.001$) (Fig. 7C). Notably, the stemness scores and proliferation potential scores were higher in ICIs-treated melanomas ($P < 0.001$), while the ITH

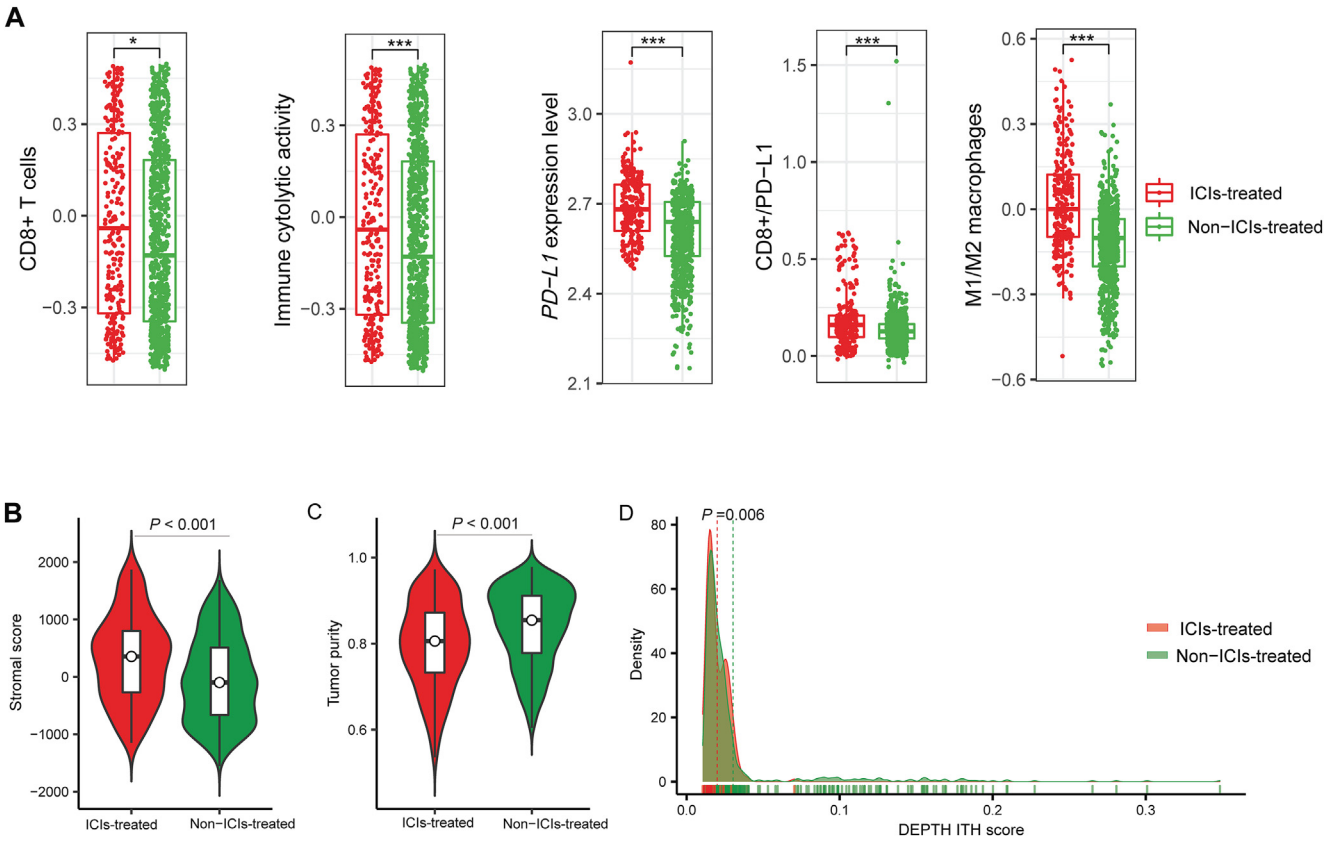

Fig. 7. Comparisons of molecular and phenotypic features between the melanomas treated and those untreated with ICIs. Comparisons of immune signatures (A), stromal signatures (B), tumor purity (C), and stemness, proliferation potential, and ITH scores (D) between ICIs-treated and non-ICIs-treated melanomas. The one-tailed Mann–Whitney *U* test or two-tailed Student's *t* test *P*-values are indicated. ITH: intratumor heterogeneity.

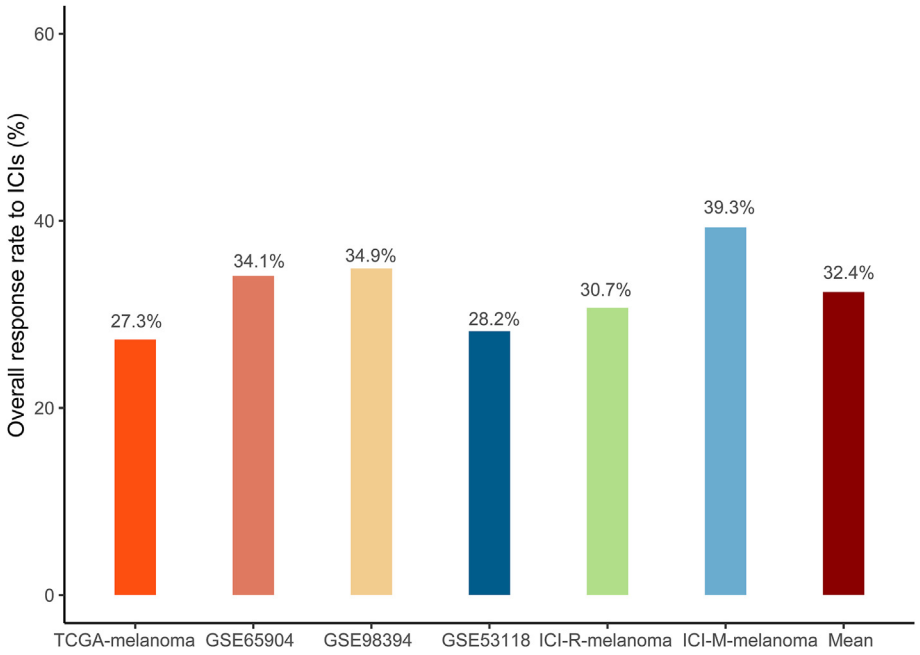

Fig. 8. Estimate of the response rate to ICIs in melanoma based on the immune subtyping in the six cohorts.

scores evaluated by the DEPTH algorithm [46] were lower in this cohort (P = 0.007) (Fig. 7D).

Taken together, these data implicate that the use of ICIs may change the characteristics of tumor cells and the TME in melanoma. These alterations in turn may influence the response to ICIs.

3.7. Evaluation of the response rate to ICIs in melanoma

In ICI-R-melanoma, the response rate to ICIs was 44.4%, 31.3%, and 18.6% in Im-H, Im-M, and Im-L, respectively, and the overall response rate was 30.7%. In ICI-M-, the response rate was 42.9%, 57.9%, and 8.0% in the three subtypes, respectively, and the overall response rate was 39.3%. By averaging the response rates in identical subtypes of both datasets, we estimated the response rate in Im-H, Im-M, and Im-L melanomas to be 45.8%, 45.3%, and 15.0%, respectively. Applying the averaged response rates in the subtypes to TCGA-melanoma, GSE65904, GSE98394, and GSE53118 in which patients were not treated by ICIs, we estimated their overall response rate was 27.3%, 34.1%, 34.9%, and 28.2%, respectively, based on the numbers of Im-H, Im-M, and Im-L melanomas in these datasets (Fig. 8). Both the mean and median overall response rates in the six groups of melanomas were equal to 32.40%. The estimated response rate to ICIs in melanoma (around 30%) based on the subtyping in the six cohorts conforms to that reported by clinical data [47].

4. Discussion

Based on the enrichment scores of 28 immune cells in the TIME, we identified three immune subtypes (Im-H, Im-M, and Im-L) of melanoma. We demonstrated the stability and producibility of this classification method in six different datasets, including four cohorts not treated with ICIs and two cohorts treated with ICIs. Im-H was characterized by strong immune signatures, low stemness and proliferation potential, genomic stability, high immunotherapy response rate, and favorable prognosis. In contrast, Im-L was characterized by weak immune signatures, high stemness and proliferation potential, genomic instability, low immunotherapy response rate, and unfavorable prognosis. The significantly different survival prognosis among these immune subtypes is attributed to significantly different anti-tumor immune response and immunotherapy response among them. Our data confirmed that the inflamed TIME can promote anti-tumor immunity and immunotherapy response in melanoma. Interestingly, as an immunosuppressive signature, PD-L1 had the highest expression levels in Im-H, which showed the strongest anti-tumor immune response among the three subtypes. One potential explanation for this observation could be that PD-L1 is also expressed on immune cells, which are the most abundant in Im-H. We provided evidence for this inference by analyzing a scRNA-seq dataset for melanoma. We found that PD-L1 had significantly higher expression levels in immune cells than in tumor cells (P < 0.001) (Fig. 9). Because Im-H has the highest levels of immune cell infiltration, it is justified that PD-L1 expression is upregulated in this subtype.

It has been shown that TMB and SCNAs have a positive and negative association with anti-tumor immune response, respectively [39]. Our analysis revealed that SCNAs had a significant impact on the TIME in melanoma and that TMB showed no significant impact (Fig. 4B). It suggests that the high level of SCNAs instead of low TMB is a major factor responsible for the low immunity in Im-L. In addition, the elevated activities of the Hippo signaling, ErbB signaling, and cell cycle pathways could also contribute to the reduced anti-tumor immunity in Im-L. In contrast, the elevated activities of the MAPK signaling, apoptosis, calcium signaling, VEGF signaling, cell adhesion molecules, focal adhesion, gap junction, and PPAR signaling pathways have potential contributions to the increased anti-tumor immunity in Im-H. In TCGA-melanoma, we identified numerous pathways highly enriched in Im-H, many of which were also upregulated in responsive versus non-responsive melanomas, such as calcium signaling, Jak-STAT signaling, MAPK signaling, VEGF signaling, and many immune-related pathways. It supports the positive association between anti-tumor immune signatures' enrichment levels and immunotherapy response. It should be noted that the calcium signaling is an important messenger in diverse cell types, including lymphocytes [48]. However, the scRNA-seq data showed that the enrichment scores of calcium signaling was significantly higher in tumor cells than in immune cells (P < 0.001) (Fig. 9). In addition, we identified five pathways highly enriched in Im-L, including adherens junction,

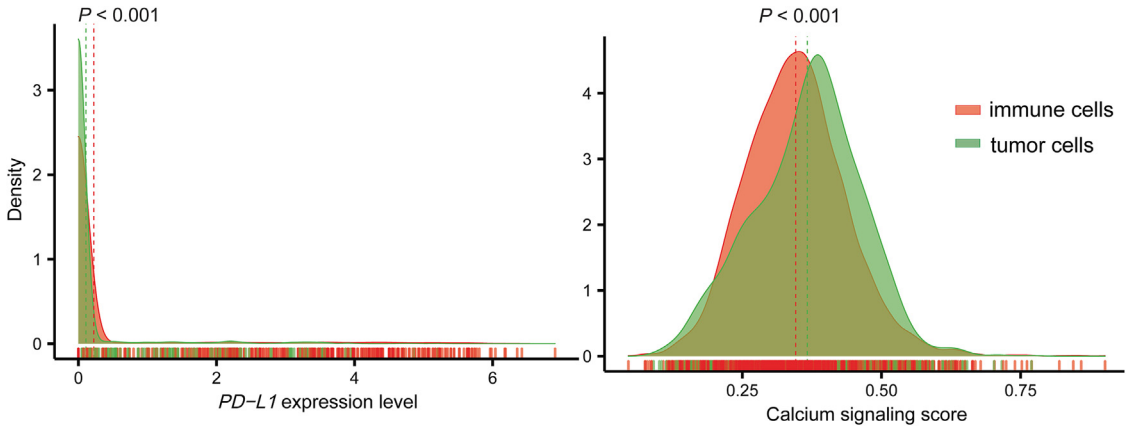

Fig. 9. Comparisons of PD-L1 expression levels and calcium signaling enrichment scores between tumor cells and immune cells in the scRNA-seq dataset (GSE72056) for cutaneous melanoma.

insulin signaling, arginine and proline metabolism, purine metabolism, and ErbB signaling. However, the activities (enrichment scores) of these pathways showed no significant difference between responsive and non-responsive melanomas. It could indicate that there is no defined association between downregulation of anti-tumor immune signatures and low immunotherapy response rate in melanoma.

We identified certain pathways showing significant positive associations with the response to ICIs in melanoma. Many of these pathways are involved in immunostimulatory signatures, such as T and B cell receptor signaling, cytokine-cytokine receptor interaction, NK cell mediated cytotoxicity, antigen processing and presentation, and chemokine signaling. It suggests that the strong immunostimulatory signature in the TIME may increase immunotherapy response in melanoma. Besides, some cancer-associated pathways, including PPAR signaling, glycolysis/gluconeogenesis, MAPK signaling, VEGF signaling, and calcium signaling, are associated with increased immunotherapy response in melanoma. The positive association between these pathways and immunotherapy response could be attributed to their promotion of the inflamed TIME in melanoma.

We found that stemness scores were significantly higher in non-responsive than in responsive melanomas, indicating that tumor stemness may promote immunotherapy resistance. The reason why tumor stemness leads to immunotherapy resistance could be attributed to that tumor stemness promotes the formation of immune-deprived TME in which ITH increases [49]. Interestingly, we found that stemness scores were significantly higher in the melanomas treated with ICIs than those untreated with ICIs. It indicates that the use of ICIs could enhance tumor stemness, and the increased tumor stemness in turn contributes to immunotherapy resistance. This hypothesis warrants further exploration.

5. Conclusions

Melanoma can be classified into three immune subtypes based on the TIME. These subtypes have significantly different prognosis and immunotherapy response. Our unsupervised machine learning method recaptures the immunological heterogeneity in melanoma and provides potential clinical implications for the immunotherapy of melanoma.

6. Availability of data and material

The TCGA-melanoma dataset was downloaded from the genomic data commons data portal (https://portal.gdc.cancer.gov/). The GSE65904, GSE98394, and GSE53118 datasets were downloaded from the NCBI gene expression omnibus (https://www.ncbi.nlm.nih.gov/geo/). The single-cell RNA sequencing (scRNA-seq) dataset (GSE72056) was downloaded from the NCBI gene expression omnibus (https://www.ncbi.nlm.nih.gov/geo/). A summary of these datasets is presented in Supplementary Table S1.

7. Ethics approval and consent to participate

Ethical approval was waived since we used only publicly available data and materials in this study.

CRediT authorship contribution statement

Qian Liu: Data curation, Formal analysis, Investigation, Software, Validation, Visualization, Writing - review & editing. **Rongfang Nie:** Formal analysis, Data curation, Visualization. **Mengyuan Li:** Data curation, Formal analysis. **Lin Li:** Software, Formal analysis. **Haiying Zhou:** Validation, Formal analysis. **Hui Lu:** Resources, Investigation, Funding acquisition, Writing - review & editing. **Xiaosheng Wang:** Conceptualization, Methodology, Resources, Investigation, Writing - original draft, Supervision, Project administration, Funding acquisition.

Funding

This work was supported by the China Pharmaceutical University (grant number 3150120001 to XW) and Zhejiang Provincial Natural Science Foundation of China (grant number LS21H060001 to HL).

Declaration of Competing Interest

The authors declare that they have no known competing financial interests or personal relationships that could have appeared to influence the work reported in this paper.

Appendix A. Supplementary data

Supplementary data to this article can be found online at https://doi.org/10.1016/j.csbj.2021.08.005.

References

[1] Del Paggio JC. Immunotherapy: Cancer immunotherapy and the value of cure. Nat Rev Clin Oncol 2018;15(5):268–70.
[2] Lugowska I, Teterycz P, Rutkowski P. Immunotherapy of melanoma. Contemp Oncol (Pozn) 2018;2018(1):61–7.

[3] Wang X, Li M. Correlate tumor mutation burden with immune signatures in human cancers. BMC Immunol 2019;20(1):4.
[4] Imbert C, Montfort A, Fraisse M, Marcheteau E, Gilhodes J, Martin E, et al. Resistance of melanoma to immune checkpoint inhibitors is overcome by targeting the sphingosine kinase-1. Nat Commun 2020;11(1). https://doi.org/10.1038/s41467-019-14218-7.
[5] Patel SP, Kurzrock R. PD-L1 Expression as a Predictive Biomarker in Cancer Immunotherapy. Mol Cancer Ther 2015;14(4):847–56.
[6] Le DT, Uram JN, Wang H, Bartlett BR, Kemberling H, Eyring AD, et al. PD-1 Blockade in Tumors with Mismatch-Repair Deficiency. N Engl J Med 2015;372(26):2509–20.
[7] Rizvi NA, Hellmann MD, Snyder A, Kvistborg P, Makarov V, Havel JJ, et al. Cancer immunology. Mutational landscape determines sensitivity to PD-1 blockade in non-small cell lung cancer. Science 2015;348(6230):124–8.
[8] Gajewski TF. The Next Hurdle in Cancer Immunotherapy: Overcoming the Non-T-Cell-Inflamed Tumor Microenvironment. Semin Oncol 2015;42(4):663–71.
[9] He Y, Jiang Z, Chen C, Wang X. Classification of triple-negative breast cancers based on Immunogenomic profiling. J Exp Clin Cancer Res 2018;37(1). https://doi.org/10.1186/s13046-018-1002-1.
[10] Xu F, Chen J-X, Yang X-B, Hong X-B, Li Z-X, Lin L, et al. Analysis of Lung Adenocarcinoma Subtypes Based on Immune Signatures Identifies Clinical Implications for Cancer Therapy. Mol Ther Oncolytics 2020;17:241–9.
[11] Akbani R, Akdemir K, Aksoy BA, Albert M, Ally A, Amin S, et al. Genomic Classification of Cutaneous Melanoma. Cell 2015;161(7):1681–96.
[12] Cirenajwis H, Ekedahl H, Lauss M, Harbst K, Carneiro A, Enoksson J, et al. Molecular stratification of metastatic melanoma using gene expression profiling: Prediction of survival outcome and benefit from molecular targeted therapy. Oncotarget 2015;6(14):12297–309.
[13] Cabrita R, Lauss M, Sanna A, Donia M, Skaarup Larsen M, Mitra S, et al. Tertiary lymphoid structures improve immunotherapy and survival in melanoma. Nature 2020;577(7791):561–5.
[14] Badal B, et al. Transcriptional dissection of melanoma identifies a high-risk subtype underlying TP53 family genes and epigenome deregulation. JCI Insight 2017;2(9).
[15] Mann GJ, Pupo GM, Campain AE, Carter CD, Schramm S-J, Pianova S, et al. BRAF mutation, NRAS mutation, and the absence of an immune-related expressed gene profile predict poor outcome in patients with stage III melanoma. J Invest Dermatol 2013;133(2):509–17.
[16] Barter RL, Schramm S-J, Mann GJ, Yang YH. Network-based biomarkers enhance classical approaches to prognostic gene expression signatures. BMC Syst Biol 2014;8(Suppl 4):S5. https://doi.org/10.1186/1752-0509-8-S4-S5.
[17] Van Allen EM, Miao D, Schilling B, Shukla SA, Blank C, Zimmer L, et al. Genomic correlates of response to CTLA-4 blockade in metastatic melanoma. Science 2015;350(6257):207–11.
[18] Hugo W, Zaretsky JM, Sun Lu, Song C, Moreno BH, Hu-Lieskovan S, et al. Genomic and Transcriptomic Features of Response to Anti-PD-1 Therapy in Metastatic Melanoma. Cell 2016;165(1):35–44.
[19] Nathanson T, Ahuja A, Rubinsteyn A, Aksoy BA, Hellmann MD, Miao D, et al. Somatic Mutations and Neoepitope Homology in Melanomas Treated with CTLA-4 Blockade. Cancer Immunol Res 2017;5(1):84–91.
[20] Riaz N, Havel JJ, Makarov V, Desrichard A, Urba WJ, Sims JS, et al. Tumor and Microenvironment Evolution during Immunotherapy with Nivolumab. Cell 2017;171(4):934–949.e16.
[21] Snyder A, Makarov V, Merghoub T, Yuan J, Zaretsky JM, Desrichard A, et al. Genetic basis for clinical response to CTLA-4 blockade in melanoma. N Engl J Med 2014;371(23):2189–99.
[22] Ulloa-Montoya F, Louahed J, Dizier B, Gruselle O, Spiessens B, Lehmann FF, et al. Predictive Gene Signature in MAGE-A3 Antigen-Specific Cancer Immunotherapy. J Clin Oncol 2013;31(19):2388–95.
[23] Tirosh I, Izar B, Prakadan SM, Wadsworth MH, Treacy D, Trombetta JJ, et al. Dissecting the multicellular ecosystem of metastatic melanoma by single-cell RNA-seq. Science 2016;352(6282):189–96.
[24] Picelli S, Faridani OR, Björklund ÅK, Winberg G, Sagasser S, Sandberg R. Full-length RNA-seq from single cells using Smart-seq2. Nat Protoc 2014;9(1):171–81.
[25] Hanzelmann S, Castelo R, Guinney J. GSVA: gene set variation analysis for microarray and RNA-seq data. BMC Bioinf 2013;14:7.
[26] Danaher P, Warren S, Lu R, Samayoa J, Sullivan A, Pekker I, et al. Pan-cancer adaptive immune resistance as defined by the Tumor Inflammation Signature (TIS): results from The Cancer Genome Atlas (TCGA). J Immunother Cancer 2018;6(1). https://doi.org/10.1186/s40425-018-0367-1.
[27] Yoshihara K et al. Inferring tumour purity and stromal and immune cell admixture from expression data. Nat Commun 2013;4:2612.
[28] Subramanian A, Tamayo P, Mootha VK, Mukherjee S, Ebert BL, Gillette MA, et al. Gene set enrichment analysis: a knowledge-based approach for interpreting genome-wide expression profiles. Proc Natl Acad Sci U S A 2005;102(43):15545–50.
[29] Kanehisa M, Furumichi M, Tanabe M, Sato Y, Morishima K. KEGG: new perspectives on genomes, pathways, diseases and drugs. Nucleic Acids Res 2017;45(D1):D353–61.
[30] Langfelder P, Horvath S. WGCNA: an R package for weighted correlation network analysis. BMC Bioinf 2008;9:559.
[31] Mermel CH, Schumacher SE, Hill B, Meyerson ML, Beroukhim R, Getz G. GISTIC2.0 facilitates sensitive and confident localization of the targets of focal somatic copy-number alteration in human cancers. Genome Biol 2011;12(4). https://doi.org/10.1186/gb-2011-12-4-r41.
[32] Knijnenburg TA et al. Genomic and Molecular Landscape of DNA Damage Repair Deficiency across The Cancer Genome Atlas. Cell Rep 2018;23(1):239–254 e6.
[33] Benjamini Y, Hochberg Y. Controlling the false discovery rate: a practical and powerful approach to multiple testing. J Royal Stat Soc B 1995;57(1):289–300.
[34] Jiang Z, Liu Z, Li M, Chen C, Wang X. Immunogenomics Analysis Reveals that TP53 Mutations Inhibit Tumor Immunity in Gastric Cancer. Transl Oncol 2018;11(5):1171–87.
[35] Lyu H, Li M, Jiang Z, Liu Z, Wang X. Correlate the TP53 Mutation and the HRAS Mutation with Immune Signatures in Head and Neck Squamous Cell Cancer. Comput Struct Biotechnol J 2019;17:1020–30.
[36] Liu Z, Li M, Jiang Z, Wang X. A Comprehensive Immunologic Portrait of Triple-Negative Breast Cancer. Transl Oncol 2018;11(2):311–29.
[37] Iakovleva NV, Gorbushin AM, Storey KB. Modulation of mitogen-activated protein kinases (MAPK) activity in response to different immune stimuli in haemocytes of the common periwinkle Littorina littorea. Fish Shellfish Immunol 2006;21(3):315–24.
[38] Jiang F, Wu C, Wang M, Wei Ke, Zhou G, Wang J. Multi-omics analysis of tumor mutation burden combined with immune infiltrates in melanoma. Clin Chim Acta 2020;511:306–18.
[39] Davoli T, Uno H, Wooten EC, Elledge SJ. Tumor aneuploidy correlates with markers of immune evasion and with reduced response to immunotherapy. Science 2017;355(6322):eaaf8399. https://doi.org/10.1126/science:aaf8399.
[40] Jung H, Kim HS, Kim JY, Sun J-M, Ahn JS, Ahn M-J, et al. DNA methylation loss promotes immune evasion of tumours with high mutation and copy number load. Nat Commun 2019;10(1). https://doi.org/10.1038/s41467-019-12159-9.
[41] Jiang Z, Liu Z, Li M, Chen C, Wang X. Increased glycolysis correlates with elevated immune activity in tumor immune microenvironment. EBioMedicine 2019;42:431–42.
[42] Janse van Rensburg HJ, Azad T, Ling M, Hao Y, Snetsinger B, Khanal P, et al. The Hippo Pathway Component TAZ Promotes Immune Evasion in Human Cancer through PD-L1. Cancer Res 2018;78(6):1457–70.
[43] Faget J, Groeneveld S, Boivin G, Sankar M, Zangger N, Garcia M, et al. Neutrophils and Snail Orchestrate the Establishment of a Pro-tumor Microenvironment in Lung Cancer. Cell Rep 2017;21(11):3190–204.
[44] Hong Z, et al. Recruitment of mismatch repair proteins to the site of DNA damage in human cells. J Cell Sci, 2008;121(Pt 19):3146-54.
[45] Goel S, DeCristo MJ, Watt AC, BrinJones H, Sceneay J, Li BB, et al. CDK4/6 inhibition triggers anti-tumour immunity. Nature 2017;548(7668):471–5.
[46] Li M, Zhang Z, Li L, Wang X. An algorithm to quantify intratumor heterogeneity based on alterations of gene expression profiles. Commun Biol 2020;3(1). https://doi.org/10.1038/s42003-020-01230-7.
[47] Leonardi G, Candido S, Falzone L, Spandidos D, Libra M. Cutaneous melanoma and the immunotherapy revolution (Review). Int J Oncol 2020;57(3):609–18.
[48] Vig M, Kinet J-P. Calcium signaling in immune cells. Nat Immunol 2009;10(1):21–7.
[49] Miranda A, Hamilton PT, Zhang AW, Pattnaik S, Becht E, Mezheyeuski A, et al. Cancer stemness, intratumoral heterogeneity, and immune response across cancers. Proc Natl Acad Sci U S A 2019;116(18):9020–9.